Journal of Materials Chemistry A

PdAg Nanoparticles Supported on Resorcinol-Formaldehyde Polymers Containing Amine Groups: The Promotional Effect of Phenylamine Moieties on CO_2 Transformation to Formic Acid

Journal:	*Journal of Materials Chemistry A*
Manuscript ID	TA-ART-03-2019-002552.R1
Article Type:	Paper
Date Submitted by the Author:	05-Jun-2019
Complete List of Authors:	Masuda, Shinya; Osaka University, a. Division of Materials and Manufacturing Science, Graduate School of Engineering Mori, Kohsuke; Osaka University, Division of Materials and Manufacturing Science Kuwahara, Yasutaka; Osaka University, Graduate School of Engineering, Division of Materials and Manufacturing Science Yamashita, Hiromi; Osaka University, Division of Materials and Manufacturing Science

ARTICLE

PdAg Nanoparticles Supported on Resorcinol-Formaldehyde Polymers Containing Amine Groups: The Promotional Effect of Phenylamine Moieties on CO_2 Transformation to Formic Acid

Received 00th January 20xx,
Accepted 00th January 20xx

DOI: 10.1039/x0xx00000x

Shinya Masuda,[a] Kohsuke Mori,*[a,b,c] Yasutaka Kuwahara[a,c] and Hiromi Yamashita*[a,c]

The transformation of CO_2 to formic acid (FA, HCOOH) is one of the most promising means of developing economically-viable CO_2-mediated energy cycles, owing to the many advantages of FA as a feedstock, hydrogen source and fuel source for fuel cells. In the present study, we synthesized a series of catalysts consisting of PdAg nanoparticles supported on resorcinol-formaldehyde polymers having various amine contents (PdAg/amine-RF). These catalysts exhibited significant activity during CO_2 hydrogenation to produce FA, especially when the support with the highest amine concentration was employed. Analyses of active Pd species using X-ray absorption fine structure (XAFS) and X-ray photoelectron spectroscopy (XPS) demonstrated the formation of Pd-N bonds in these materials, and oxidized nitrogen, phenylmethanimine, phenylimine and phenylamine moieties were identified based on N 1s XPS data. Density functional theory calculations showed that the adsorption energy of bicarbonate ions on the PdAg alloy is much higher in close proximity to phenylamine molecules, while the activation energy of the rate determining step is significantly lower. These predictions are in good agreement with the experimental results, which demonstrate that the reaction order associated with the bicarbonate concentration is decreased with increasing nitrogen concentration in the catalyst. A significant correlation was observed between the turnover number and the nitrogen content (attributed to the presence of phenylamine moieties) estimated from both XPS and elemental analysis, indicating that phenylamine groups made the most significant contribution toward the promotion of this reaction.

Introduction

Carbon dioxide (CO_2) is a greenhouse gas that has significant impacts on climate change and ocean acidification.[1, 2] The continued use of fossil fuels as an energy source means that anthropogenic CO_2 will be emitted into the Earth's atmosphere for the foreseeable future. As a means of mitigating the effects of such emissions, the transformation of CO_2 into useful chemical products such as hydrocarbons (e.g., methane, ethane) and alcohols (e.g., methanol, ethanol) has been widely studied.[3-9] This transformation not only reduces the emission of CO_2, but also supplies valuable chemical and fuel resources, and so developing an economical CO_2-mediated energy cycle is a promising aspect of addressing future life.[10]

Formic acid (FA), the simplest CO_2 hydrogenation product, is a useful feedstock chemical and can also serve as a hydrogen source for fuel cells.[11-13] FA functions as a superior hydrogen storage compound because it is highly stable, relatively nontoxic, has a high hydrogen storage capacity (4.4 wt%) and is a liquid under ambient conditions. FA can be employed as an energy carrier during a CO_2-mediated energy cycle because it decomposes to hydrogen and CO_2.[14-16] In addition, FA has received much attention as a potential fuel source for direct liquid fuel cell systems.[17] FA is typically synthesized by methyl formate hydrolysis or biomass oxidation,[18, 19] but the development of catalysts for the production of FA via CO_2 hydrogenation would be highly beneficial in terms of satisfying the increasing demand for this compound.

The gas phase hydrogenation of CO_2 to generate FA has a positive free energy change (CO_2 (g) + H_2 (g) → HCOOH (l), ΔG = +33 kJ mol^{-1}). In aqueous solution, the reaction proceeds more readily because of the relatively low activation energy (CO_2 (aq) + H_2 (aq) → HCOOH (aq), ΔG = −4 kJ mol^{-1}).[20] The thermodynamic equilibrium can also be shifted to the product side by adding a weak base, such as a tertiary amine or alkali/alkaline earth bicarbonate (CO_2 (aq) + H_2 (aq) + B → HCO_2^- (aq) + BH^+ (B: base), ΔG = −35.4 kJ mol^{-1}). In addition, significant progress has been made in the transformation of CO_2 to FA utilizing homogeneous systems based on Ir or Ru complexes that function in aqueous media.[21-26] Heterogeneous systems using catalysts loaded with Au or Pd metal nanoparticles (NPs) have also been reported.[27-33] However, such heterogeneous systems still require high catalyst concentrations, elevated pressures and the use of organic solvents, and so the development of highly active heterogeneous systems would be an improvement.

Our group has previously reported heterogeneous systems capable of generating FA in aqueous media.[10, 34-36] In this prior research, we investigated the role of Ag alloyed with Pd. The presence of Ag was effectively increased the adsorption step of bicarbonate in the FA synthesis and affected the electronic state of Pd, resulting in the acceleration of rate-determining step and dramatically improved the activity. In addition to that, we determined that catalysts made of PdAg alloy NPs supported on a phenylamine-modified mesoporous

[a] Division of Materials and Manufacturing Science, Graduate School of Engineering, Osaka University, 2-1 Yamadaoka, Suita, Osaka 565-0871, Japan. E-mail: K. M. mori@mat mat.eng.osaka-u.ac.jp; H. Y. yamashita@mat.eng.osaka-u.ac.jp; Fax: +81-6-6879-7457; Tel: +81-6-6879-7457
[b] JST, PRESTO, 4-1-8 Honcho, Kawaguchi, Saitama, 332-0012, Japan.
[c] Unit of Elements Strategy Initiative for Catalysts Batteries (ESICB), Kyoto University, Katsura, Kyoto 615-8520, Japan.

† Footnotes relating to the title and/or authors should appear here.
Electronic Supplementary Information (ESI) available: [details of any supplementary information available should be included here]. See DOI: 10.1039/x0xx00000x

carbon exhibited high catalytic activity during FA synthesis, and that the phenylamine present in the support played an important role in improving the activity.[36] However, the nitrogen content in this material could not be readily adjusted, based on the intrinsic difficulty in performing amine functionalization. In addition, the relationship between amine modification of the support and the catalytic activity of the Pd was not fully elucidated.

In the work reported herein, we produced a series of catalysts comprising PdAg NPs supported on polymers containing amine groups, based on a typical resorcinol-formaldehyde resin synthesis procedure. These materials were subsequently utilized as catalysts for the CO_2 hydrogenation reaction to produce FA, and exhibited significant activity, especially when supports with high amine contents were employed. The relationship between activity and nitrogen content was determined. Density functional theory (DFT) calculations were also performed to clarify the role of the amine moiety in enhancing the bicarbonate adsorption process as well in promoting the rate-determining step.

Experimental

Materials

Resorcinol, formaldehyde solution (37%), silver nitrate, ammonium hydroxide (28%), sodium borohydride ($NaBH_4$), sodium hydrogen carbonate ($NaHCO_3$) and ethanol were purchased from Nakalai Tesque, Inc. Sodium tetrachloropalladate (II) and 4,6-diaminoresorcinol dihydrochloride were obtained from Tokyo Chemical Industry Co., Ltd.

General procedure for synthesis of amine containing resorcinol-formaldehyde (amine-RF) polymer

Amine containing resorcinol formaldehyde (amine-RF) support was synthesized by the typical procedure of RF resin.[37] Resorcinol (R) and 4,6-diaminoresorcinol dihydrochloride (AR) were added into ethanol (40 mL) and distilled water (100 mL) mixture solution. Total mol amount of R and AR was fixed as 4.54 mmol and the ratio of R:AR were changed to 10:0, 3:7, 5:5, 7:3 and 0:10 to prepare the RF, amine-RF3, amine-RF5, amine-RF7 and amine-RF10, respectively. After 10 min sonication, ammonium hydroxide was added to adjust the solution pH around 9.0, followed by adding formaldehyde aqueous solution (0.5 mL). The mixture was stirred 24 h and finally collected by centrifugation washed with ethanol. Then, it was dried under vacuum overnight.

Synthesis of PdAg nanoparticles supported amine-RF catalysts (PdAg/amine-RF)

Each support (0.2 g) was mixed with distilled water (50 mL) and stirred. Then, sodium tetrachloropalladate (II) (Na_2PdCl_4, 19.0 μmol) and silver nitrate ($AgNO_3$, 19.0 μmol) were added into the mixture and stirred additional 1 h. After stirring, the solution was evaporated and redispersed to the distilled water (50 mL). Finally, the specimen was reduced with $NaBH_4$ ($NaBH_4$/metal (mol) = 10) and collected by filtration, and washed several times carefully. Then, it was dried under vacuum overnight.

Characterization

Powder X-ray diffraction (XRD) patterns were recorded using a Rigaku Ultima IV diffractometer with Cu Kα radiation (λ=1.54056 Å). Transmission electron microscope (TEM) images were obtained with a Hitachi HF-2000 FE-TEM operated at 200 kV. Nitrogen adsorption-desorption isotherms were measured at -196 °C using BELSORP-max system (MicrotracBEL Corp.). Samples were degassed at 120 °C for 3 h under vacuum to vaporize the physisorbed water. Specific surface area was calculated by BET (Brunauer-Emmett-Teller) method using nitrogen adsorption data ranging from p/p_0=0.05 to 0.35. Infrared spectra were obtained with a JASCO FTIR-6100. Samples were diluted with KBr and compressed into thin disk-shaped pellets. Quantification of loading amount of amine functionality in specimens was performed by the elemental analysis using a MICRO CORDER JM-10 (J-SCIENCE LAB CO., Ltd.). CO pulse adsorption was performed by using a BEL-METAL-1 instrument (BEL Japan, Inc.) to measure the amount of surface exposed Pd. The samples were pretreated under a helium flow at 50 °C for 15 min, and subsequently under a H_2 flow at 100 °C for 60 min. The CO adsorption was measured at 50 °C at a CO flow rate of 20 mL・min^{-1} X-ray photoelectron spectroscopy (XPS) was performed with Shimadzu ESCA-3400 system. Mg Kα X-ray radiation ($h\nu$ = 1253.6 eV) was used as the excitation source. The binding energy of the spectra was calibrated using C 1s core level for the contaminant at 284.5 eV. Pd and Ag K-edge X-ray absorption fine structure (XAFS) spectra were recorded by using a fluorescenceyield collection technique at the beam line 01B1 station with an attached Si(111) monochromator at SPring-8, JASRI, Harima, Japan (prop. No. 2017B1081, 2017B1084). The data reduction was performed by using the REX2000 program (Rigaku).

Measurement of CO_2 adsorption capacity

CO_2 gas adsorption experiments were performed under dry conditions by thermogravimetric (TG) analysis using TG-DTA system (Rigaku, Thermo plus EVO2). The sample (10 mg) was loaded into a alumina pan and heated at 120 °C for 180 min with a heating rate of 10 °C min^{-1} under a N_2 flow (100 mL min^{-1}) to remove the physisorbed water. Then, the temperature was lowered to 30 °C and kept for 60 min in a flow of N_2 (100 mL min^{-1}) to stabilize the sample weight and temperature. The amount of adsorbed CO_2 was monitored for 30 min under a flow of 10 % CO_2 containing N_2 (total 100 mL min^{-1}).

Catalytic hydrogenation of CO_2

CO_2 hydrogenation to produce FA was conducted using a batch reactor system (stainless autoclave (60 mL)). After the addition of disodium succinate (external standard), the yield of FA was determined by HPLC using a Shimadzu HPLC instrument equipped with a Bio-Rad Aminex HPX-87H Ion Exclusion Column (300 mm×7.8 mm). 5 mm H_2SO_4 (0.500 mL min^{-1}) was used as a mobile phase. TON values were determined according to

TON =[produced FA after 24 h]/[moles of total Pd]

Recycling test of hydrogenation of CO_2 to obtain FA

Recycling test of FA production was conducted using the same methods above. After the each reaction, catalyst was centrifuged and washed twice with water. Then, the catalyst was redispersed to $NaHCO_3$ aqueous solution and used for the next reaction.

DFT calculation

All DFT calculations were performed with the $DMol_3$ program in Materials Studio 17.2. The generalized gradient approximation (GGA) exchange-correlation functional proposed by Perdew, Burke, and Ernzerhof (PBE) was combined with the double numerical basis set plus polarization functions (DNP) with a cutoff value of 4.0 Å. Brillouin zone integrations were performed on a Monkhorst–Pack k-point grid with 2 × 2 × 1 = 4 points as a, b and c axis.[38] We adopted the medium level for integration grid. Three atomic surface layers (111) consisting of a 5 × 5 PdAg alloy (lattice constant : 3.988 Å) unit cells with periodic boundary conditions was chosen as a model of alloy, where the bottom two layers were fixed at the corresponding bulk position and the top layer was allowed to relax during geometry optimizations.

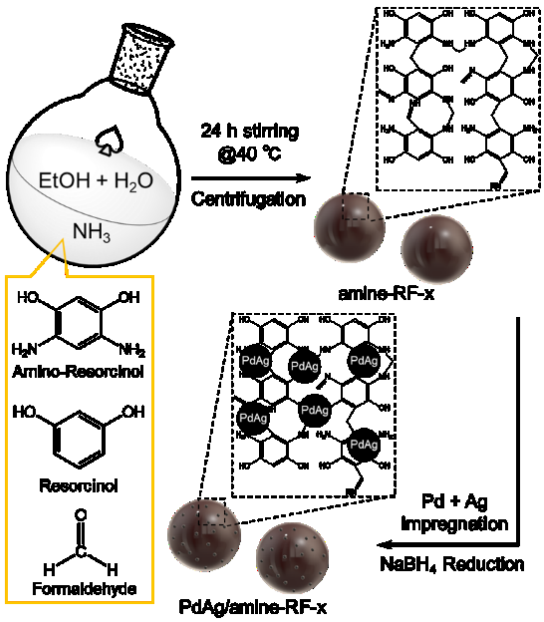

Scheme 1 An illustration summarizing the synthesis of PdAg NPs supported on a resorcinol-formaldehyde polymer containing amine groups (amine-RF) catalysts.

The slab was separated by a vacuum space with a height of 20 Å. In addition, phenylamine, phenylmethanimine and phenylamine were used as a model of base without fixing. The adsorption energy E_{ad} is defined as $E_{ad} = E_{adsorbate} + E_{slab+amine} - E_{adsorbate/slab+amine}$ in which $E_{adsorbate}$ is the total energy of free adsorbate, $E_{slab+amine}$ is the total energy of the bare slab and amine moiety and $E_{adsorbate/slab+amine}$ is the total energy of the adsorbate–slab+amine system.

Results and discussion

Characterization

The procedure used to prepare a catalyst consisting of PdAg NPs on an amine-containing resorcinol-formaldehyde support (amine-RF) is shown in scheme 1 and described in detail in the Experimental section.[37] Briefly, varying amounts of resorcinol (R) and 4,6-diaminoresorcinol hydrochloride (AR) were dissolved in a mixture of water and ethanol by sonication, after which an ammonium hydroxide solution (28 %) was added to adjust the pH to approximately 9, followed by a reaction with formaldehyde to generate the amine-RF support. This support was impregnated with the Pd and Ag precursors and then reduced with $NaBH_4$. The resulting materials are referred to herein as amine-RFx, where x is the amount of AR (0, 3, 5, 7, 10) as the ratio of R:AR (10:0, 7:3, 5:5, 3:7, 0:10) during the preparation.

The carbon, hydrogen, and nitrogen proportions in the samples were determined by elemental analysis (Table 1), and the data show that the N content was increased with increasing the ratio of AR. The N content of the specimen prepared using only resorcinol (termed RF) indicated that ammonia was also incorporated into this support during the preparation process, possibly based on a reaction of ammonia with formaldehyde.

Fig. S1 presents the Fourier transform infrared (FT-IR) spectra of the RF, amine-RF3, amine-RF5, amine-RF7 and amine-RF10 specimens. Each support produced peaks attributed to $-CH_2-$ and $-CH_3$ bonds at approximately 2850 and 2920 cm^{-1} and peaks due to C=O bonds at approximately 2340 and 2370 cm^{-1}. However, only the amine-RF spectra contained peaks attributed to N–H bonds at approximately 1550 cm^{-1}. The intensity of these peaks also increased with increasing the ratio of AR. The RF support should show a small peak due to the N-H bond at around 1550 cm^{-1}. But, we cannot observe the corresponding peak because of the overlapping by the major two peaks. The other reason is due to the formation of carbocation species by the reaction between amine (NH_3) and aldehyde through the Mannich reaction, which attacks the resorcinol to form RF polymer. According to this reaction mechanism, most of N-H bond will disappear during the synthesis.

The specific surface areas of various supports were calculated from nitrogen adsorption-desorption isotherms (Fig. S2) by the BET method, and the textual properties of these materials are summarized in Table 1. The supports containing less AR showed higher surface areas and pore volumes, and these values of the support with highest AR ratio were lower than those of the RF specimen. This trend can be explained based on considering the morphologies of the various supports (Fig. S3-S7). All supports showed a spherical particle morphology, especially the RF specimen, in which the particles were well separated. However, the particle size of the RF support was obviously larger than those of the amine-RF specimens, which decreased its surface area. In addition, in the case of the materials containing AR, the particles showed greater aggregation as the ratio of AR was increased. This in turn decreased the surface area in the specimens having higher AR levels.

Fig. S8 shows the X-ray diffraction (XRD) patterns of the catalysts made of PdAg supported on amine-RF polymers. The minor peak produced only by the specimens having lower AR concentrations, at 38°, is attributed to Ag metal. No peaks originating from metallic Pd or PdAg are observed, indicating the formation of small Pd or PdAg NPs. The average particle sizes were estimated from transmission electron microscopy (TEM) images of the various specimens, and are provided in Table 1. The diameters of the NPs were smaller in the catalysts containing higher proportions of AR, suggesting that there were interactions between the amine groups and metal precursors during the preparation process.[14]

Fourier transform extended X-ray absorption fine structure (FT-

Table 1 The C, H and N proportions in the samples as determined by elemental analysis, textual properties of each supports obtained from nitrogen adsorption-desorption isotherms and average diameter of PdAg NPs determined from TEM images.

Sample	Content [wt%]			Surface area (S_{BET})	Pore volume (V_P)	PdAg NPs size
	H	C	N	[$m^2 \cdot g^{-1}$]	[$cm^3 \cdot g^{-1}$]	[nm]
RF	5.6	58.6	5.6	10.1	0.044	4.8
amine-RF3	5.2	54.6	8.3	28.5	0.106	3.1
amine-RF5	5.0	53.8	10.3	20.5	0.087	3.1
amine-RF7	4.9	51.2	11.9	12.1	0.050	2.9
amine-RF10	4.8	48.3	14.1	8.9	0.035	2.3

EXAFS) data were acquired to investigate the effects of surface amine groups on the local structures of the Pd and Ag species. The Pd K-edge X-ray absorption near edge structure (XANES) spectra of each specimen resemble that of PdO (Fig. S9). In the case of the lower AR specimens, the FT-EXAFS spectra show two sharp peaks (Fig. 1(A)) at 2.5 Å (ascribed to metallic Pd-Pd bonds) and at 1.5 Å (ascribed to Pd-O or Pd-N bonds). However, the Pd-Pd peak intensity gradually decreased as the AR proportion was increased, and the PdAg/amine-RF10 catalyst produced only a single sharp peak at approximately 1.5 Å without any metallic peak. This result confirms that the peak at 1.5 Å primarily originated from Pd-N bonds. Each of the Ag K-edge spectra exhibit a single peak at approximately 2.7 Å, ascribed to metallic Ag-Ag bonds. This result also supports the formation of Pd-N bonds, since it is unlikely that only Pd species were oxidized without the oxidation of Ag species, given that the oxidation of Ag is easier because the redox potential of Ag ($Ag^+ + e^- \rightarrow Ag$: $E_0 = 0.799$ vs. RHE) is lower than that of Pd ($Pd^{2+} + 2e^- \rightarrow Pd$: $E_0 = 0.915$ vs. RHE).

Fig. 1(B) also shows that the presence of Ag metallic bonds was gradually decreased in the catalysts containing more AR, indicating the formation of smaller particles. This agrees with the trend observed in the TEM images. These images show numerous metal NPs with average particle diameters of roughly 2.3 nm in the case of the PdAg/amine-RF10 catalyst (Table 1). However, the Pd K-edge FT-EXAFS spectrum of the PdAg/amine-RF10 contains only an insignificant metallic Pd peak. If only NPs having an average diameter of approximately 2.3 nm were formed on the amine-RF10 support, a metallic Pd peak should appear in the spectrum.[39] Therefore, this result indicates that some of the Pd species were present as atomic-level Pd sites in the vicinity of nitrogen atoms, in the form of Pd clusters or single Pd atoms.[40, 41] These species cannot be observed by TEM because of resolution limitations. CO adsorption analyses of the PdAg/amine-RF10 also provided evidence for the formation of such species (Table S1). In these trials, the material did not adsorb any CO prior to hydrogen reduction and, even after reduction at 100 °C, only a very small amount of CO was adsorbed. From these data, the average Pd particle size was estimated to be 73.5 nm, which is not

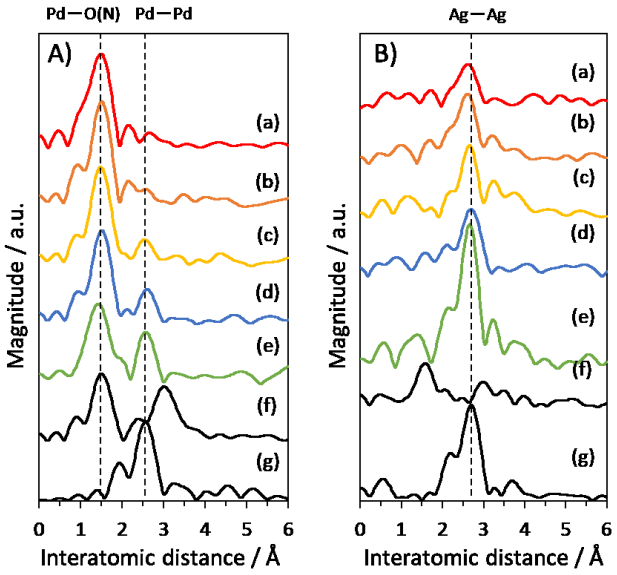

Fig. 1 (A) Pd K-edge FT-EXAFS spectra of (a) PdAg/amine-RF10, (b) PdAg/amine-RF7, (c) PdAg/amine-RF5, (d) PdAg/amine-RF3, (e) PdAg/RF, (f) PdO and (g) Pd foil specimens. (B) Ag K-edge FT-EXAFS spectra of (a) PdAg/amine-RF10, (b) PdAg/amine-RF7, (c) PdAg/amine-RF5, (d) PdAg/amine-RF3, (e) PdAg/RF, (f) AgO and (g) Ag foil specimens.

Table 2 The proportion of each nitrogen moiety estimated from XPS measurement for various supports.

	Oxidized N	Phenylamine	Phenylmethanimine	Phenylimine
RF	29.0	29.5	26.4	15.1
amine-RF3	13.9	25.4	35.7	25.0
amine-RF5	12.0	26.6	38.1	23.4
amine-RF7	9.8	22.8	39.5	27.9
amine-RF10	6.9	25.2	42.3	25.6

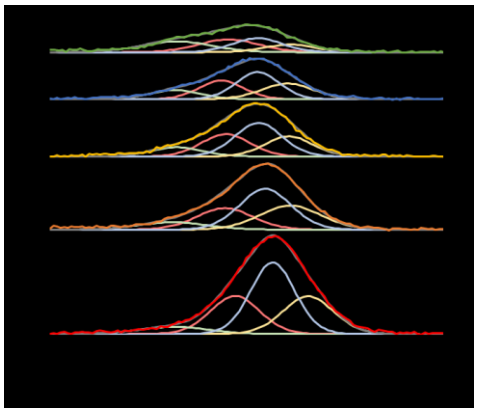

Fig. 2 N 1s orbital XPS spectra of (a) PdAg/amine-RF10, (b) PdAg/amine-RF7, (c) PdAg/amine-RF5 and (d) PdAg/amine-RF3, (e) PdAg/RF specimens.

consistent with the TEM images. Thus, we believe that nitrogen atoms in the vicinity of the Pd species inhibited the adsorption of CO, owing to the formation of Pd-N bonds.

The electronic properties of Pd, Ag and N in these materials were investigated using XPS analysis. The Pd 3d XPS spectra (Fig. S11) demonstrate that Pd species were present as both Pd^0 and Pd^{2+}, while the majority of the Ag species existed as Ag^0, based on the Ag 3d XPS spectra (Fig. S12). These observations are in good agreement with the XAFS results, and support the formation of Pd–N bonds. The electronic state of the Pd was gradually shifted to lower binding energies in samples with higher AR contents and also the spectrum of PdAg/amine-RF10 was shifted to lower binding energy compared to that of Pd/amine-RF10 (Fig. S13), indicating the formation of electron-rich Pd species because of both amine amount and alloying effect with Ag. In addition, the N 1s XPS spectrum of each specimen (Fig. 2) contains a large, broad peak derived from various nitrogen species. Judging from the precursors employed in the synthetic procedure and fitting of the spectra, it is evident that the amine-RF supports primarily contained four types of nitrogen moieties: oxidized N, a primary amine (phenylamine), a secondary aldimine (phenylmethanimine) and a primary aldimine (phenylimine).[42-45] The proportion of each nitrogen moiety is summarized in Table 2.

Formic Acid Generation through the Hydrogenation of CO_2 with H_2

The catalytic hydrogenation of CO_2 with H_2 to produce FA was assessed in an autoclave using a 1.0 M aqueous $NaHCO_3$ solution at pH 8.5 under a total pressure of 2.0 MPa (H_2:CO_2 = 1:1, volume ratio) at 100 °C. Fig. 3 shows the turnover number (TON) values obtained from each specimen after a 24 h reaction (calculated based on the Pd loading amount as determined by inductively coupled plasma (ICP, Table S1)), together with the average diameters of PdAg NPs determined from TEM images. The activities were evidently improved as the nitrogen content was increased, and the catalyst

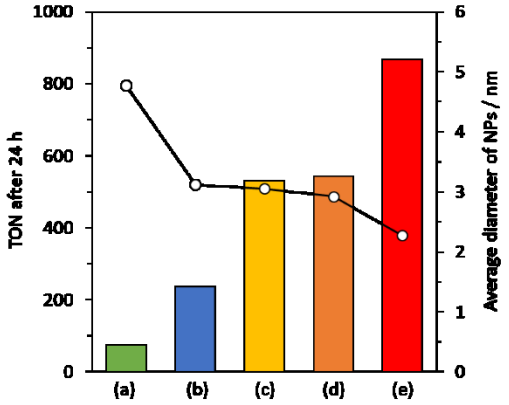

Fig. 3 Comparison of TON values measured at 24 h for produced FA on the basis of the total amount of Pd during the hydrogenation of CO_2 and average diameter of the NPs over (a) PdAg/RF, (b) PdAg/amine-RF3, (c) PdAg/amine-RF5, (d) PdAg/amine-RF7 and (e) PdAg/amine-RF10. Reaction conditions: catalyst (10 mg), $NaHCO_3$ in aqueous solution (1.0 M, 15 mL) and total pressure of 2.0 MPa (CO_2:H_2 = 1:1, volume ratio) at 100 °C for 24 h.

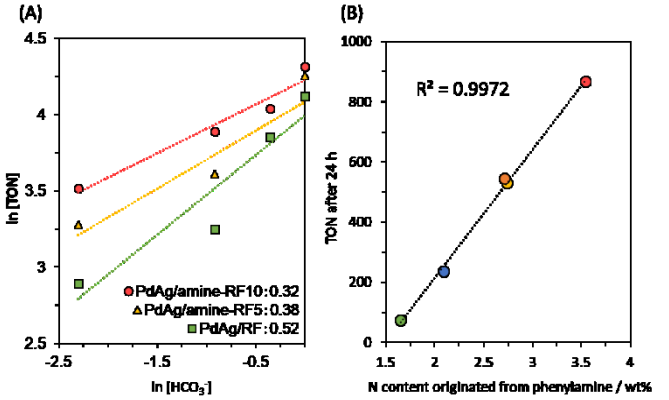

PdAg/amine-RF5 and PdAg/RF. Reaction conditions: catalyst (10 mg), $NaHCO_3$ in aqueous solution (1.0 M, 15 mL) and total pressure of 2.0 MPa (CO_2:H_2 = 1:1, volume ratio) at 100 °C for 2 h. (B) The relationship between the TON during FA synthesis and the nitrogen content attributed to phenylamine specie estimated from XPS results (Table 2) of each catalysts.

synthesized using only AR as the precursor showed the highest catalytic activity, with a TON of 867. This value was almost equivalent to that obtained from our previously reported PdAg/amine-modified mesoporous carbon catalyst, which demonstrated high activity under low pressure conditions.[36] The TON of the PdAg/amine-RF10 was more than ten times higher than that of the monometallic Pd/amine-RF10 catalyst (TON=73). This drastic enhancement of activity is ascribed to the synergic effect by alloying of Pd with Ag, because the activity of monometallic Ag is negligible. The PdAg/amine-RF10 catalyst showed a 30% loss of catalytic activity when reused in a second reaction (Fig. S14). However, ICP analysis demonstrated that no Pd had leached into the reaction solvent (that is, no Pd above the detection limit of 1 ppm). There was no further significant loss in activity during a third reaction, indicating that only a portion of the catalyst was destroyed during the first reaction, and that deactivation was primarily due to mass loss. This consideration was supported by the XPS and TEM analysis of used PdAg/amine-RF10 catalyst. Pd 3d XPS results showed there are no clear deference in the electronic state of Pd after reaction, but the proportion of Pd^{2+}/Pd^0 was changed (Figure S15). This is because the reaction atmosphere is highly reducible, that is 1 MPa of hydrogen pressure and 100 °C. Thus, some of Pd^{2+} cations were reduced to Pd^0 during the reaction. TEM analysis also showed the particle sizes of PdAg NPs and support morphology were almost not changed (NPs size: 2.3 nm to 2.4 nm after reaction).

In addition, the PdAg/amine-RF10 catalyst showed high activity (with a TON of 63 and a turnover frequency (TOF) of 2.6 h^{-1}) during direct CO_2 hydrogenation to formic acid in the absence of an additive to the reaction solution (water) at 40 °C under a total pressure of 4 MPa (H_2:CO_2 = 1:1, volume ratio) after 24 h. In spite of the relatively low total pressure conditions employed, the activity demonstrated by the PdAg/amine-RF10 was equal to or greater than those recently reported for other heterogeneous catalyst systems, including PdNi/CNT (TOF = 0.2 h^{-1}, H_2/CO_2 = 25/25 [bar]),[46] 0.6Pd/g-C_3N_4 (TOF = 1.5 h^{-1}, H_2/CO_2 = 25/25 [bar])[47] and 2Pd/ECN (Exfoliated Carbon Nitride) (TOF = 2.3 h^{-1}, H_2/CO_2 = 25/25 [MPa]),[48] as summarized in Table S2. This system also does not require the addition of a base, allows ready separation of the product and uses pure water, and so represents an ideal environmentally-benign chemical process for FA synthesis with potential industrial applications.

The high activity of this material can possibly be explained by considering the Pd XPS spectra, which shows that the Pd became more electron-rich as the amine content was increased. We previously identified a correlation between the formation rate of FA and the Pd 3d binding energy as determined by XPS, in which electron-rich species showed better catalytic activity.[34] Judging from these findings, a similar effect occurred in the present study. That is, an electron-rich Pd state enhanced the catalytic effect. We also confirmed the Effect of Pd^{2+}/Pd^0 ratio, however, there are no correlation between the activity and Pd^{2+}/Pd^0 ratio (Table S3).

The formation of small NPs is another possible reason for the improved catalytic activity, but no correlation was found between the particle size and the catalytic activity (Fig. S17). In contrast, a correlation between the nitrogen content of the support and the catalytic activity was confirmed, indicating that nitrogen species either affected the Pd activity or promoted the catalysis (Fig. S18).

In addition, the effect of the bicarbonate concentration was greatly dependent on the total nitrogen amount (Fig. 4 (A)). The reaction order was found to increase in the order of PdAg/RF (0.52) < PdAg/amine-RF5 (0.38) < PdAg/amine-RF10 (0.32), in agreement with the catalytic activity. In addition to this result, the amount of CO_2 adsorbed on the amine-RF10 specimen was 0.15 mmol/g, which was 1.5 times higher than that adsorbed on the RF specimen (0.10 mmol/g) (Table S4). These results suggest that the step involving bicarbonate was the rate-determining process in this reaction, and that a higher amine group concentration in the catalyst promoted this step.

Here, we propose a likely mechanism for the action of the nitrogen species in the support. As noted, the amine-RF supports contained four different types of nitrogen moieties. In order to investigate the differences between these, bicarbonate adsorption energies (E_{ad}) were determined using DFT calculations (Fig. 5 (A)). In the present trials, bicarbonate ions were generated under basic conditions via the dissolution of CO_2. During the DFT calculations, phenylamine, phenylmethanimine and phenylimine were used as the models of each nitrogen moiety and the PdAg alloy structure was modeled with three atomic surface layers (111) consisting of 5 × 5 PdAg alloy surface unit cells with periodic boundary conditions. The nitrogen atom of each amine was adsorbed on 3-atom ensemble site between two Pd and one Ag atoms with the distance of approximately 3.84 Å,

Fig. 4 (A) Reactivity dependence on HCO_3^- concentration of PdAg/amine-RF10,

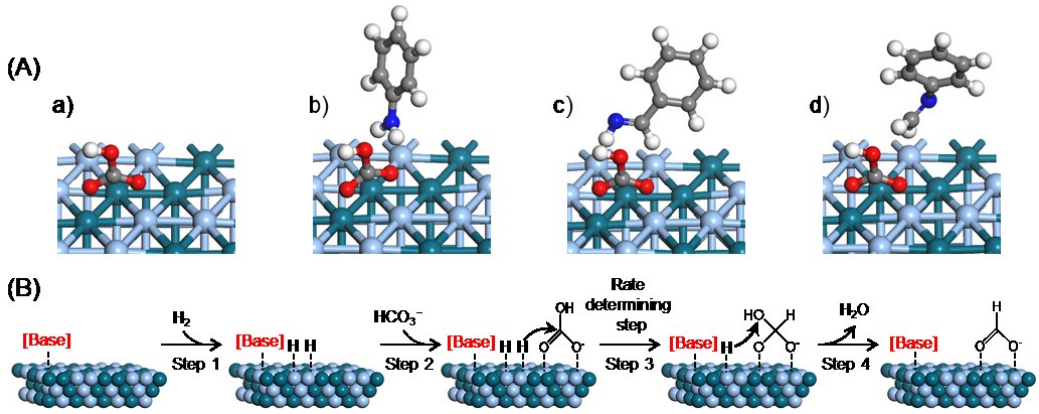

Fig. 5 (A) The optimized model for the calculations of adsorption energy of bicarbonate(HCO_3^-) (a) without amine, (b) with the Phenylamine molecule, (c) with the Phenylmethanimine molecule and (d) with the Phenylimine molecule and (B) the schematic mechanism of FA formation on the PdAg alloy with base presence.

Table 3. (A) Adsorption energy of bicarbonate ion (HCO_3^-) and (B) activation energy of the nucleophilic attack of H atom on the C atom of bicarbonate ion (rate determining step) calculated on the three atomic surface layers (111) consisting of a 5 × 5 PdAg alloy surface unit cells with periodic boundary conditions (a) without amine, (b) with the Phenylamine molecule, (c) with the Phenylmethanimine molecule and (d) with the Phenylimine molecule.

Specimens		(A) Adsorption Energy of HCO_3^- [kJ/mol]	(B) Activation Energy (Step 3) Nucleophilic attack of H to HCO_3^- [kJ/mol]
a)	PdAg	172.0	300.0
b)	PdAg + Phenylamine	192.7	156.2
c)	PdAg + Phenylmethanimine	176.1	200.1
d)	PdAg + Phenylimine	176.0	259.6

4.82 Å and 3.88 Å in the case of phenylamine, phenylimine and phenylmethanimine, respectively (Fig. S19). Note that, phenylimine showed longer distance than other moieties because of the steric effects. Moreover, the surface charges of Pd and Ag atoms were changed because of the charge transfer from amine moiety (Fig. S20), but the Pd and Ag atoms in bottom layer were almost not changed, indicating only surface PdAg alloy was affected by amine moiety. As a result, E_{ad} was estimated to be 176.1 and 176.0 kJ/mol when phenylmethanimine or phenylimine were located in the vicinity of the PdAg alloy model, respectively, both of which are close to the E_{ad} of 172.0 kJ/mol for a pure PdAg alloy surface without amine molecules. However, the E_{ad} value with the phenylamine was calculated to be 192.7 kJ/mol, which is significantly higher than those for the other molecules (Table 3). These results demonstrate that the phenylamine moiety has the most positive effect with regard to the adsorption of bicarbonate.

We previously proposed a mechanism for the formation of FA on PdAg NPs based on experimental and theoretical results (Fig. 5 (B)).[34, 36] In this mechanism, hydrogen is initially dissociated at a Pd site on the PdAg alloy surface to form a Pd-hydride species. A bicarbonate ion adsorbs on the PdAg in the second step, followed by the nucleophilic attack of the H atom on the C atom of the bicarbonate ion as the third step. Finally, formate is generated, accompanied by the elimination of water through the attack of the second hydride H atom on the non-coordinated O atom. Energetically, the reduction of the bicarbonate ion is more likely to occur as the result of an attack by an active H on the C atom of the bicarbonate ion rather than on one of the O atoms. We also found that the third step (nucleophilic attack of the H atom on the C atom) has the highest activation energy (E_a) during the CO_2 transformation to FA. The E_a for the rate-determining third step was subsequently determined using the PdAg alloy model while changing the type of amine (Table 3), and the values in the presence of phenylmethanimine and phenylimine were estimated to be 200.1 and 259.6 kJ/mol, respectively. These values are both lower than that for pure PdAg alloy (300.0 kJ/mol) without amine molecules. Moreover, the E_a in the presence of phenylamine was substantially lowered (156.2 kJ/mol), indicating that the phenylamine moiety not only promotes the adsorption of bicarbonate ions, but also enhances the rate-determining step. These results indicate the importance of having phenylamine groups in close proximity to the PdAg alloy during this reaction. The presence of Pd-phenylamine species was confirmed in the Pd FT-EXAFS and XPS data, both of which provide evidence for the formation of Pd-N bonds. In addition, a significant correlation was evident ($R^2 = 0.997$) between the TON during FA synthesis and the nitrogen content (attributed to phenylamine) estimated from both XPS and elemental analysis (Fig. 4 (B)). Thus, we can conclude that nitrogen species, especially phenylamine, in close approximately to the PdAg alloy significantly promote the adsorption and hydrogenation of bicarbonate, which in turn improves the catalytic activity during the synthesis of FA.

Conclusions

Catalysts comprising PdAg NPs supported on a resorcinol-formaldehyde polymer containing amine groups demonstrated high catalytic activity during the hydrogenation of CO_2 in aqueous media to produce FA. The PdAg/amine-RF10 sample, synthesized solely using the AR precursor and formaldehyde showed the best catalytic

activity. The electron-rich state of Pd in those materials having higher amine levels was at least partly responsible for their superior catalytic activity. This effect was based on the presence of nitrogen groups on phenyl rings in the support. The effect of the bicarbonate concentration in the reaction solution was also reduced in the case of those materials having higher amine concentrations. DFT calculations showed that the bicarbonate adsorption energy was greatly increased, while the activation energy for bicarbonate hydrogenation (the rate determining step) was obviously decreased, on the PdAg alloy surface when in close proximity to phenylamine groups. The formation of Pd-N bonds was confirmed by Pd FT-EXAFS and XPS spectra. Additionally, a significant correlation was found between the TON and the nitrogen content attributed to phenylamine groups, as determined from both XPS and elemental analysis. These results demonstrate that amine groups on phenyl rings had the greatest promotional effect during this reaction, and provide information useful to the future development of nitrogen-based catalysts for the hydrogenation of CO_2 to FA.

Conflicts of interest

There are no conflicts to declare.

Acknowledgements

The present work was supported by JST-PRESTO (grant no. JPMJPR1544). Support was also provided by Grants-in-Aid for Scientific Research (nos. 26220911, 25289289, 26630409 and 26620194) from the Japan Society for the Promotion of Science (JSPS) and MEXT.

Notes and references

1. T. R. Knutson and R. E. Tuleya, *J. Clim.*, 2004, **17**, 19.
2. J. Hansen, M. Sato, R. Ruedy, K. Lo, D. W. Lea and M. M.-Elizade, *Proc. Natl. Acad. Sci. U. S. A.*, 2006, **103**, 6.
3. A. Taheri Najafabadi, *Int. J. Energy Res.*, 2013, **37**, 485-499.
4. X.-M. Liu, G. Q. Lu, Z.-F. Yan and J. Beltramini, *Ind. Eng. Chem. Res.*, 2003, **42**, 6518-6530.
5. X. Xiaoding and J. A. Moulijn, *Energy Fuels*, 1996, **10**, 305-325.
6. M. Aresta, A. Dibenedetto and A. Angelini, *Chem. Rev.*, 2014, **114**, 1709-1742.
7. A. M. Appel, J. E. Bercaw, A. B. Bocarsly, H. Dobbek, D. L. DuBois, M. Dupuis, J. G. Ferry, E. Fujita, R. Hille, P. J. A. Kenis, C. A. Kerfeld, R. H. Morris, C. H. F. Peden, A. R. Portis, S. W. Ragsdale, T. B. Rauchfuss, J. N. H. Reek, L. C. Seefeldt, R. K. Thauer and G. L. Waldrop, *Chem. Rev.*, 2013, **113**, 6621-6658.
8. E. V. Kondratenko, G. Mul, J. Baltrusaitis, G. O. Larrazábal and J. Pérez-Ramírez, *Energy Environ. Sci.*, 2013, **6**, 3112-3135.
9. Z. Ma and M. D. Porosoff, *ACS Catal.*, 2019, **9**, 2639-2656.
10. K. Mori, T. Taga and H. Yamashita, *ACS Catal.*, 2017, **7**, 3147-3151.
11. A. K. Singh, S. Singh and A. Kumar, *Catal. Sci. Technol.*, 2016, **6**, 12-40.
12. D. Mellmann, P. Sponholz, H. Junge and M. Beller, *Chem. Soc. Rev.*, 2016, **45**, 3954-3988.
13. M. Grasemann and G. Laurenczy, *Energy Environ. Sci.*, 2012, **5**, 8171-8181.
14. K. Mori, M. Dojo and H. Yamashita, *ACS Catal.*, 2013, **3**, 1114-1119.
15. K. Mori, H. Tanaka, M. Dojo, K. Yoshizawa and H. Yamashita, *Chem. Eur. J.*, 2015, **21**, 12085-12092.
16. K. Mori, K. Naka, S. Masuda, K. Miyawaki and H. Yamashita, *ChemCatChem*, 2017, **9**, 3456-3462.
17. S. Uhm, H. J. Lee and J. Lee, *Phys. Chem. Chem. Phys.*, 2009, **11**, 9326-9336.
18. W. Wang, M. Niu, Y. Hou, W. Wu, Z. Liu, Q. Liu, S. Ren and K. N. Marsh, *Green Chem.*, 2014, **16**, 2614-2618.
19. J. Xu, H. Zhang, Y. Zhao, Z. Yang, B. Yu, H. Xu and Z. Liu, *Green Chem.*, 2014, **16**, 4931-4935.
20. S. Moret, P. J. Dyson and G. Laurenczy, *Nat. Commun.*, 2014, **5**, 4017.
21. Y. Himeda, N. Onozawa-Komatsuzaki, H. Sugihara and K. Kasuga, *J. Am. Chem. Soc.*, 2005, **127**, 13118-13119.
22. T. J. Schmeier, G. E. Dobereiner, R. H. Crabtree and N. Hazari, *J. Am. Chem. Soc.*, 2011, **133**, 9274-9277.
23. S. Enthaler, J. von Langermann and T. Schmidt, *Energy Environ. Sci.*, 2010, **3**, 1207-1217.
24. R. Tanaka, M. Yamashita and K. Nozaki, *J. Am. Chem. Soc.*, 2009, **131**, 14168-14169.
25. J. F. Hull, Y. Himeda, W. H. Wang, B. Hashiguchi, R. Periana, D. J. Szalda, J. T. Muckerman and E. Fujita, *Nat. Chem.*, 2012, **4**, 383-388.
26. K. Sordakis, C. Tang, L. K. Vogt, H. Junge, P. J. Dyson, M. Beller and G. Laurenczy, *Chem. Rev.*, 2018, **118**, 372-433.
27. Q. Liu, X. Yang, L. Li, S. Miao, Y. Li, Y. Li, X. Wang, Y. Huang and T. Zhang, *Nat. Commun.*, 2017, **8**, 1407.
28. J. H. Lee, J. Ryu, J. Y. Kim, S.-W. Nam, J. H. Han, T.-H. Lim, S. Gautam, K. H. Chae and C. W. Yoon, *J. Mater. Chem. A*, 2014, **2**.
29. D. Preti, C. Resta, S. Squarcialupi and G. Fachinetti, *Angew. Chem. Int. Ed.*, 2011, **50**, 12551-12554.
30. G. H. Gunasekar, K. Park, K.-D. Jung and S. Yoon, *Inorg. Chem. Front.*, 2016, **3**, 882-895.
31. A. Alvarez, A. Bansode, A. Urakawa, A. V. Bavykina, T. A. Wezendonk, M. Makkee, J. Gascon and F. Kapteijn, *Chem. Rev.*, 2017, **117**, 9804-9838.
32. D. A. Bulushev and J. R. H. Ross, *Catalysis Reviews*, 2018, **60**, 566-593.
33. N. Onishi, M. Iguchi, X. Yang, R. Kanega, H. Kawanami, Q. Xu and Y. Himeda, *Adv. Energy Mater.*, 2018, DOI: 10.1002/aenm.201801275.
34. K. Mori, T. Sano, H. Kobayashi and H. Yamashita, *J. Am. Chem. Soc.*, 2018, **140**, 8902-8909.
35. K. Mori, S. Masuda, H. Tanaka, K. Yoshizawa, M. Che and H. Yamashita, *Chem. Commun.*, 2017, **53**, 4677-4680.
36. S. Masuda, K. Mori, Y. Futamura and H. Yamashita, *ACS Catal.*, 2018, **8**, 2277-2285.
37. J. Liu, S. Z. Qiao, H. Liu, J. Chen, A. Orpe, D. Zhao and G. Q. Lu, *Angew. Chem. Int. Ed.*, 2011, **50**, 5947-5951.
38. H. J. Monkhorst and J. D. Pack, *Physical Review B*, 1976, **13**, 5188-5192.
39. G. Vile, D. Albani, M. Nachtegaal, Z. Chen, D. Dontsova, M. Antonietti, N. Lopez and J. Perez-Ramirez, *Angew. Chem. Int. Ed.*, 2015, **54**, 11265-11269.
40. O. Y. Podyacheva, D. A. Bulushev, A. N. Suboch, D. A. Svintsitskiy, A. S. Lisitsyn, E. Modin, A. Chuvilin, E. Y. Gerasimov, V. I. Sobolev and V. N. Parmon, *ChemSusChem*, 2018, **11**, 3724-3727.
41. A. Han, W. Chen, S. Zhang, M. Zhang, Y. Han, J. Zhang, S. Ji, L. Zheng, Y. Wang, L. Gu, C. Chen, Q. Peng, D. Wang and Y. Li, *Adv. Mater.*, 2018, **30**, 1706508.
42. Y. Hu, N. Goodeal, Y. Chen, A. M. Ganose, R. G. Palgrave, H. Bronstein and M. O. Blunt, *Chem. Commun.*, 2016, **52**, 9941-9944.
43. M. Y. Hua, C. J. Chen, H. C. Chen, R. Y. Tsai, W. Cheng, C. L. Cheng and Y. C. Liu, *Sensors*, 2011, **11**, 5873-5885.
44. J. Yue and A. J. Epstein, *Macromolecules*, 1991, **24**, 4441-4445.
45. D. A. Bulushev, M. Zacharska, E. V. Shlyakhova, A. L. Chuvilin, Y. Guo, S. Beloshapkin, A. V. Okotrub and L. G. Bulusheva, *ACS Catal.*, 2015, **6**, 681-691.
46. L. T. M. Nguyen, H. Park, M. Banu, J. Y. Kim, D. H. Youn, G. Magesh, W. Y. Kim and J. S. Lee, *RSC Advances*, 2015, **5**, 105560-105566.
47. H. Park, J. H. Lee, E. H. Kim, K. Y. Kim, Y. H. Choi, D. H. Youn and J. S. Lee, *Chem Commun (Camb)*, 2016, **52**, 14302-14305.
48. C. Mondelli, B. Puertolas, M. Ackermann, Z. Chen and J. Perez-Ramirez, *ChemSusChem*, 2018, **11**, 2859-2869.

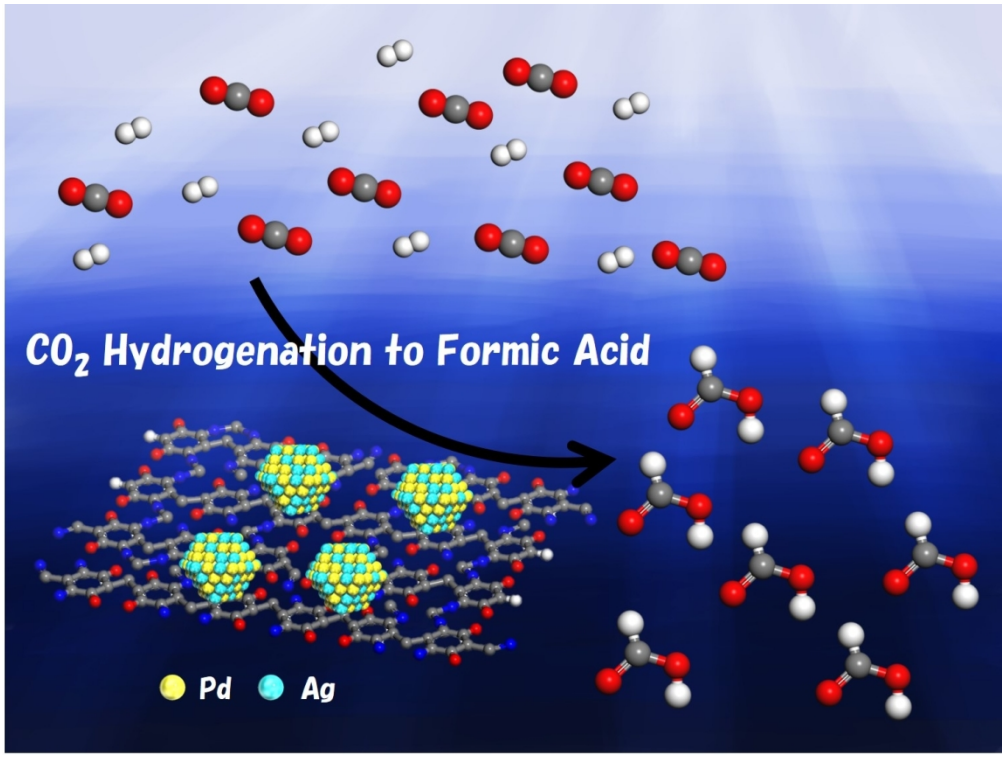

254x191mm (150 x 150 DPI)